Check for updates

NANO · MICRO small
www.small-journal.com

NIR-II Photoacoustic Reporter for Biopsy-Free and Real-Time Assessment of Wilson's Disease

*Qinrui Fu, Jiamin Ye, Juejun Wang, Naishun Liao, Hongjuan Feng, Lichao Su, Xiaoguang Ge, Huanghao Yang, and Jibin Song**

Wilson's disease (WD) is a rare inherited disorder of copper metabolism with pathological copper hyperaccumulation in some vital organs. However, the clinical diagnosis technique of WD is complicated, aggressive, and time-consuming. In this work, a novel ratiometric photoacoustic (PA) imaging nanoprobe in the NIR-II window is developed to achieve noninvasive, rapid, and accurate Cu^{2+} quantitative detection in vitro and in vivo. The nanoprobe consists of Cu^{2+}-responsive IR970 dye and a nonresponsive palladium-coated gold nanorod (AuNR-Pd), achieving a concentration-dependent ratiometric PA_{970}/PA_{1260} signal change. The urinary Cu^{2+} content is detectable within minutes down to a detection limit of 76×10^{-9} M. This report acquisition time is several orders of magnitude shorter than those of existing detection approaches requiring complex procedure. Moreover, utilizing the ratiometric PA nanoprobe, PA imaging enables biopsy-free measurement of the liver Cu^{2+} content and visualization of the liver Cu^{2+} biodistribution of WD patient, which avoid the body injury during the clinical Cu^{2+} test using liver biopsy method. The NIR-II ratiometric PA detection method is simple and noninvasive with super precision, celerity, and simplification, which holds great promise as an alternative to liver biopsy for clinical diagnosis of WD.

1. Introduction

Wilson's disease (WD) is an inherited copper (Cu) metabolic disorder caused by ATP7B gene mutations. The etiology of WD is mainly attributed to the Cu accumulation in different organs, such as liver, brain, and eye, which lead to tissue lesions due to the involvement of redox-active Cu in the generation of reactive oxygen species and the increase of oxidative stress. In particular, excess Cu^{2+} enrichment in the liver could result in various liver diseases, such as liver injury or inflammation, decompensated cirrhosis, fatty liver, etc.[1] Moreover, the content of Cu^{2+} in the urine from WD patients is also higher than the standard value (0–100 μg/24 h). Timely diagnosis and regulation of Cu^{2+} homeostasis is essential for WD patients before serious tissue damage occurs. Therefore, it is very meaningful to develop a noninvasive, highly sensitive, and reliable Cu^{2+} detection technique for WD diagnosis and subsequent healthcare decision making.

Currently, inductively coupled plasma (ICP) and atomic absorption spectrometry (AAS) are commonly used Cu^{2+} detection methods for WD patients in clinic. However, these detection methods require complicated procedures, skilled labor, and they are not suitable for in vivo detection. Although liver biopsy is applied to detect liver Cu^{2+} in clinic, this method is invasive, expensive, and dangerous. In addition, some optical probes have been developed for in vitro and in vivo detection of Cu^{2+} in WD, while challenges still remain due to the fact that they are either limited to the detection of biofluids in vitro[2,3] or only applied to the surface or near surface of living body, given limited light penetration depth.[4] Photoacoustic (PA) imaging techniques, on the other hand, integrate the advantages of optical imaging and ultrasonic imaging to achieve high spatial resolution and excellent tissue penetration depth (centimeter depths).[5,6] Especially PA imaging in the second near-infrared (NIR-II) window possesses deeper tissue penetration and higher signal-to-background ratio.[7,8] Based on these advantages, PA imaging techniques with excellent functional probe is more suitable for in vivo bioimaging and disease detection.[9–12] Yet the conventional intensity-dependent PA amplitude detection is susceptible to some insensitive artifacts such as changes in PA probe concentration and target analyte size, local light deposition, and photobleaching.[13] Ratiometric PA detection, which can improve sensing specificity, sensitivity, and accuracy, has been reported to displace simplex PA signal detection.[14–17] However, only a limited number of ratiometric PA probes have been developed for specific detection of abnormal metal ions-related diseases.[18–20] Moreover, to the best of our knowledge, there is no report of an activatable ratiometric PA probe in the NIR-II window for rapid, quantitative, noninvasive detection of urinary Cu^{2+} and liver Cu^{2+} of WD. Therefore, it is urgent to develop a simple, time-saving, visual, and highly sensitive method that can act as an alternative to the current clinical detection methods such as ICP and liver biopsy for the WD diagnosis.

Herein, we designed an activatable NIR-II ratiometric PA imaging probe (AuNR-Pd@PIR970/PEG), in which gold

Q. Fu, J. Ye, J. Wang, N. Liao, H. Feng, L. Su, X. Ge, Prof. H. Yang, Prof. J. Song
MOE Key Laboratory for Analytical Science of Food Safety and Biology
Institution, College of Chemistry
Fuzhou University
Fuzhou 350108, P. R. China
E-mail: jibinsong@fzu.edu.cn

The ORCID identification number(s) for the author(s) of this article can be found under https://doi.org/10.1002/smll.202008061.

DOI: 10.1002/smll.202008061

 © 2021 Wiley-VCH GmbH

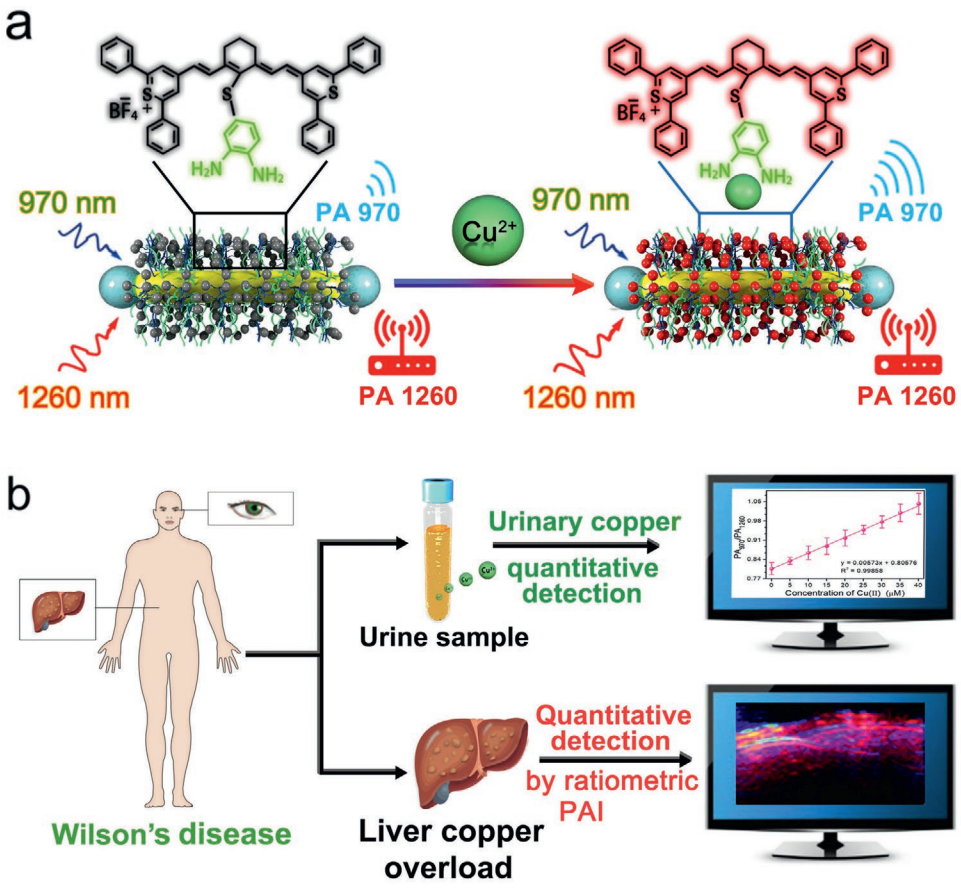

Figure 1. Illustration of a) design of Cu^{2+}-responsive ratiometric photoacoustic probe (AuNR-Pd@PIR970/PEG). b) Urinary Cu^{2+} quantitative detection and ratiometric in vivo liver bioimaging for WD patients, using AuNR-Pd@PIR970/PEG as detection probe.

nanorod-Pd (AuNR-Pd) composite was coated with Cu^{2+}-responsive molecule IR970 (4-[2-[2-[3,4-diamiobenzenethiol]-3-[(2,6-diphenyl-4*H*-thiopyran-4-ylidene)ethylidene]-1-cyclohexen-1-yl] ethenyl]-2,6-diphenylthiopyrylium), for quantitative detection of urinary Cu^{2+} and in vivo visualization of liver Cu^{2+} in WD. As shown in **Figure 1**, AuNR-Pd@PIR970/PEG nanoprobe consisted of NIR PA contrast reagent (IR970) that was selectively reactive to Cu^{2+} and inert inorganic AuNR-Pd with strong absorption peak at 1260 nm, thus achieving ratiometric PA (PA_{970}/PA_{1260}) detection of Cu^{2+}. Using PA_{970}/PA_{1260} as an indicator, AuNR-Pd@PIR970/PEG could quantitatively detect the content of urinary Cu^{2+} and enable the tracing of the in vivo liver Cu^{2+} distribution of WD mice by 3D PA imaging. The ratiometric PA imaging based on the activatable NIR-II nanoprobe is a promising technique that can serve as an alternative to current clinical methods due to their noninvasion, sensitivity, rapidity, and visualization.

2. Results and Discussion

To prepare the AuNR-Pd@PIR970/PEG nanoprobe, the AuNR-Pd were first prepared by enabling palladium nanoparticles (Pd) anchored at a tip of AuNR according to our previously reported method.[21] The average length and width of AuNR-Pd were ≈60.2 and 8.3 nm, respectively, and the aspect ratio was 7.25 (**Figure 2**a,b and Figure S1, Supporting Information). Interestingly, compared to AuNR, the coating of Pd resulted in obvious red-shift in the NIR-II window (Figure S2, Supporting Information), which was desirable for the in vivo PA imaging with deeper tissue penetration. IR970 were synthesized by linking the 3,4-diamiobenzenethiol (Figure S3, Supporting Information) with 4-[2-[2-chloro-3-[(2,6-diphenyl-4*H*-thiopyran-4-ylidene) ethylidene]-1-cyclohexen-1-yl] ethenyl]-2,6-diphenylthiopyrylium tetrafluoroborate (IR-1061). The structure of the IR970 was characterized by ^{1}H NMR (Figure S4, Supporting Information). To prepare the activatable NIR-II ratiometric PA nanoprobe AuNR-Pd@PIR970/PEG, AuNR-Pd was grafted with mixed hydrophilic thiolated polyethylene glycol (PEG-SH, M_W = 50 kDa) and thiolated poly(acrylic acid) (PAA-SH, M_W = 12 kDa) through covalent Au−S bond (AuNR-Pd@PAA/PEG). The coated PEG brushes provided enhanced hydrophilicity for improving circulation in living system and PAA brushes provided sufficient carboxyl groups to conjugate IR970. In the following, the AuNR-Pd@PIR970/PEG nanoprobe was synthesized by conjugating IR970 on the grafted PAA through covalent amide bond (Figure 2a). Compared with AuNR-Pd, their morphology of the AuNR-Pd@PIR970/PEG showed virtually no change (Figure 2c). Furthermore, we also measured the size of AuNR-Pd, AuNR-Pd@PAA/PEG, and

© 2021 Wiley-VCH GmbH

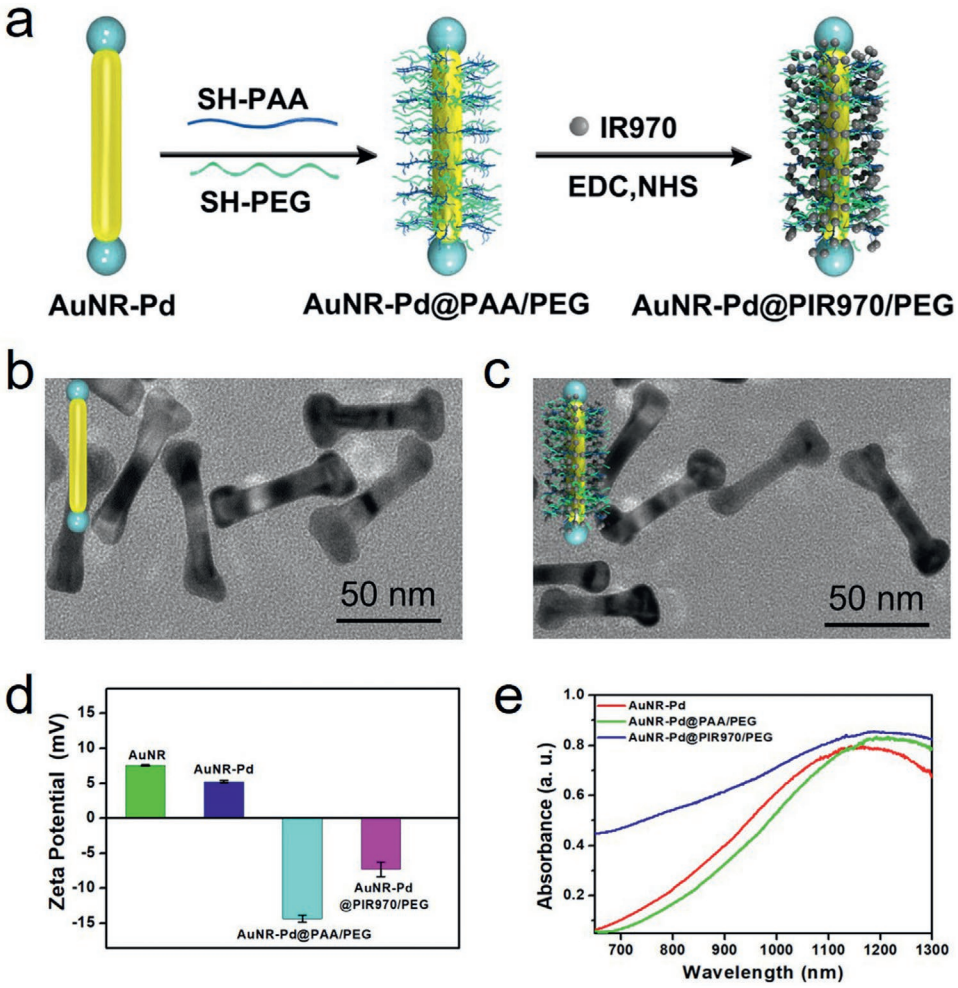

Figure 2. a) Preparation path of AuNR-Pd@PIR970/PEG nanoprobe. b) Transmission electron microscope (TEM) of AuNR-Pd. c) TEM of AuNR-Pd@PIR970/PEG nanoprobe. d) Zeta potential of AuNR, AuNR-Pd, AuNR-Pd@PAA/PEG, and AuNR-Pd@PIR970/PEG. e) UV-vis–NIR spectrum of AuNR-Pd, AuNR-Pd@PAA/PEG, and AuNR-Pd@PIR970/PEG.

AuNR-Pd@PIR970/PEG nanoparticles by dynamic light scattering analysis (Figure S5, Supporting Information), which indicated that there was only a slight increase in the particle size before and after loading of IR970 on the AuNR-Pd. The zeta potential of the AuNR-Pd@PAA/PEG was changed from 5.22 to –14.37 mV, indicating the PEG and PAA with negative charge were successfully conjugated on the AuNR-Pd surface. Meanwhile, the zeta potential of the as-prepared AuNR-Pd@P(IR970)/PEG was –7.31, because the IR970 reacted with the carboxyl group of PAA (Figure 2d). In addition, the UV-vis–NIR spectrum showed the maximum peak of AuNR-Pd at ≈1150 nm and showed near 50 nm red-shift following PEG and PAA grafted, due to the increase of negative charge on the surface of AuNR-Pd reduced the frequency of plasmon resonance (Figure 2e). These results revealed the successful loading of IR970 on the AuNR-Pd with efficiency of 67.8%.

Prior to the investigation for the Cu^{2+}-responsive property of the AuNR-Pd@PIR970/PEG, the mechanism of IR970 in response to Cu^{2+} was first studied. The IR970 precursor (IR-1061) had a small highest occupied molecular orbital–lowest unoccupied molecular orbital band gap, leading to its strong absorption in the NIR window. When the electron-rich 4-mercaptophenylenediamine fragment was introduced into the IR-1061 molecule, the intramolecular charge transfer was generated, which greatly diminished its NIR absorption at 970 nm. Once the amino groups on 4-mercapto-phenyl-phenylenediamine chelated with Cu^{2+}, the electrons on the electron-rich fragments were transferred to Cu^{2+}, breaking the charge transfer process in organic dyes, thus restoring the properties of NIR absorption at 970 nm (Figure S6, Supporting Information).[22,23] Upon addition of Cu^{2+}, the absorption at 970 nm was significantly enhanced within seconds (Figure S7, Supporting Information). In order to verify the specific toward Cu^{2+}, other metal ions such as Fe^{3+}, Fe^{2+}, Na^{+}, K^{+}, Ca^{2+}, Mg^{2+}, Mn^{2+}, Zn^{2+} were added into IR970 solutions, respectively, while no obvious absorption changes at 970 nm were observed (Figure S8, Supporting Information). Taken together, these results indicated that IR970 dyes can serve as a sensing for the detection of Cu^{2+} with high selectivity and sensitivity. When IR970 was covalently linked to the AuNR-Pd surface, the obtained nanoprobe (AuNR-Pd@PIR970/PEG) was also highly selective for Cu^{2+} (Figure S9, Supporting Information).

© 2021 Wiley-VCH GmbH

Based on the excellent responsiveness of IR970 to Cu^{2+}, we further evaluated changes in the absorption spectra in response to Cu^{2+} (**Figure 3**a). As shown in Figure 3b, the absorption peak of the AuNR-Pd@PIR970/PEG nanoprobe at 970 nm increased with the increase of Cu^{2+} concentration, while the absorption at 1260 nm of AuNR-Pd remained almost the same. Subsequently, PA imaging signals at 970 and 1260 nm of the nanoprobe treated with different concentrations of Cu^{2+} were recorded, respectively. It was shown that the PA_{970} increased as a function of the Cu^{2+} concentration, while the PA_{1260} was almost unchanged (Figure 3c,d and Figure S10, Supporting Information). It was noteworthy that the ratio of PA_{970}/PA_{1260} increased significantly and a wide linear correlation with Cu^{2+} concentration ranging from 0 to 6×10^{-3} M was plotted (Figure 3e). The limit of detection was calculated to be 76×10^{-9} M, which is comparable to that of previous literature reports.[9,22] These results demonstrated that AuNR-Pd@PIR970/PEG could effectively coordinate to Cu^{2+}, and UV-vis–NIR spectrum at 970 nm

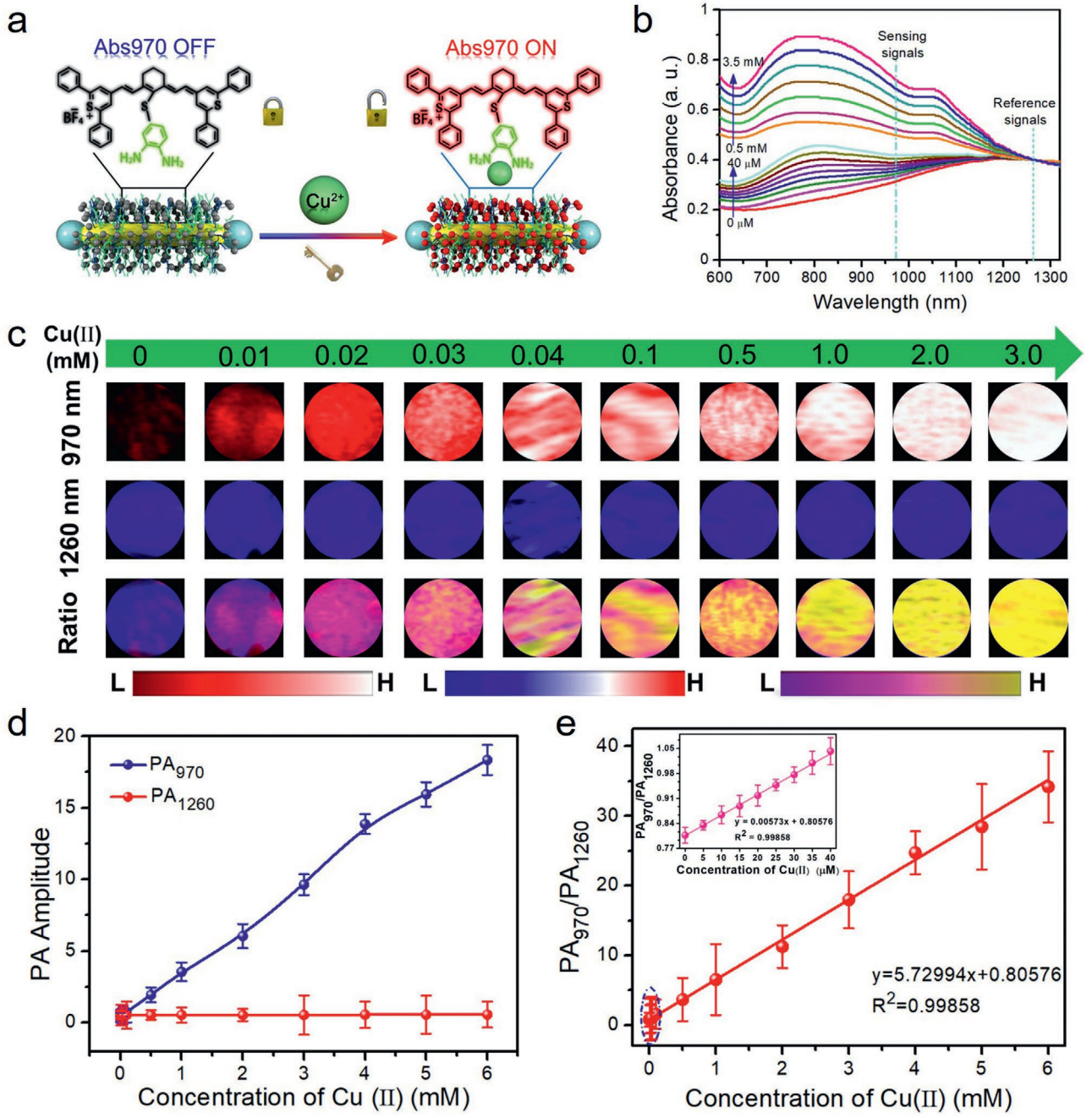

Figure 3. a) Scheme of the absorbance change of the Cu^{2+}-responsive AuNR-Pd@PIR970/PEG nanoprobe. b) UV-vis spectrum of nanoprobe in different concentration of Cu^{2+}. c) PA imaging of nanoprobe dispersed in different concentration of Cu^{2+}. d) The PA amplitude of nanoprobe treated with different concentration Cu^{2+}. e) PA_{970}/PA_{1260} signal ratios of nanoprobe measured under various concentration of Cu^{2+}.

© 2021 Wiley-VCH GmbH

transited from off to on status within a few seconds. Therefore, the AuNR-Pd@PIR970/PEG could be employed as a reliable NIR-II ratiometric nanoprobe for rapid, quantitative detection of Cu^{2+}.

WD patients usually present high levels of Cu^{2+} in urine, hence, quantitatively detecting the levels of Cu^{2+} excreted in urine within 24 h is a valuable approach for the diagnosis of WD. First, urinary Cu^{2+} content was quantitatively detected in WD mice urine samples using AuNR-Pd@PIR970/PEG as ratiometric probe by PA imaging techniques (**Figure 4**a). WD mice model was established by mutation of the gene that encodes the copper transporter ATP7B protein (The Jackson Laboratory, USA), ATP7B gene mutations resulted in the overload of Cu^{2+} in the urine and liver. The PA_{970} and PA_{1260} of 14 weeks old healthy mice and WD mice were recorded, and corresponding PA_{970}/PA_{1260} ratio value were 0.8309 and 0.9182, respectively (Figure 4b,c). According to the PA_{970}/PA_{1260} ratio value, the levels of urinary Cu^{2+} in the healthy and WD mice were 4.39×10^{-6} M (281 μg) and 19.63×10^{-6} M (1256 μg), respectively, which were consistent with the standard urinary Cu^{2+} content by ICP technique measurement.[2,24]

Encouraged by the promising result of mice urinalysis, we further quantitatively detected Cu^{2+} in human clinical urine samples via ratiometric PA imaging techniques (Figure 4d). We recorded the PA_{970}/PA_{1260} value of three groups of healthy people and WD patient urine samples with the treatment of AuNR-Pd@PIR970/PEG nanoprobe, respectively (Figure 4e,f), and the urinary Cu^{2+} contents were calculated according to the PA_{970}/PA_{1260} ratio value. The concentration of urinary Cu^{2+} for WD patients were 336.0, 247.7, and 397.3 μg/24 h, respectively; yet the concentration of urinary Cu^{2+} for healthy people were 26.9, 35.2, and 76.5 μg/24 h, respectively. To verify the accuracy of the test results by ratiometric PA imaging, we further performed medical laboratory tests on human urine using AAS technique (Figure S11, Supporting Information). The medical laboratory testing report results were consistent with the results by the ratiometric PA imaging technique (Figure 4g and Figure S12, Supporting Information). Small differences were due to the AAS data reflected the total contents of Cu, not just the Cu^{2+} content. Compared to the AAS, PA imaging technique has the advantages of simple operation flow and rapidity (completed

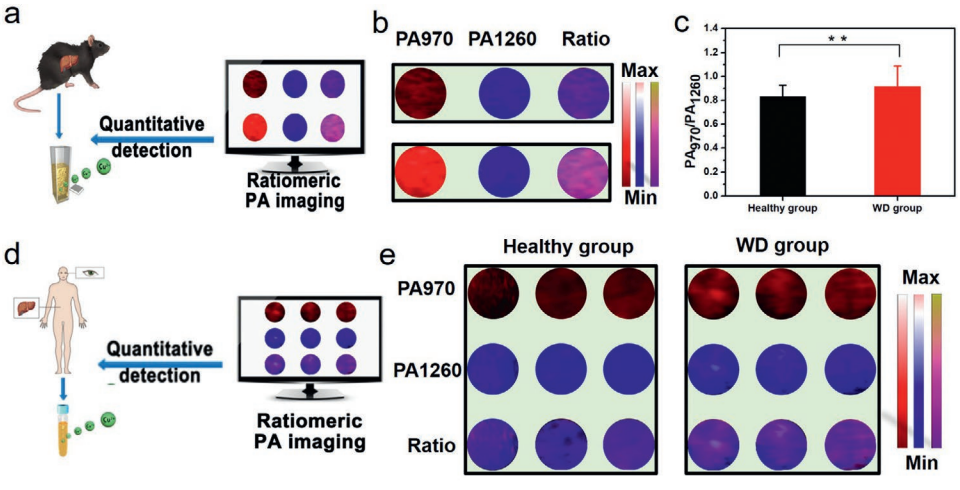

g

Methods	WD group (μg/24h)			Healthy group (μg/24h)		
Medical Laboratory Testing Report	376.0	262.5	414.1	30.0	38.4	83.7
Ratiometric PA Imaging	336.0	247.7	397.3	26.9	35.2	76.5

h

Methods	Normal people	Asymptomatic children	WD patient
In clinic	< 40 μg/24h	40-100 μg/24h	> 100 μg/24h
PA ratio	< 0.809	0.809-0.815	> 0.815

Figure 4. a) Schematic illustration of quantitative detection of mice urinary Cu^{2+} by ratiometric PA imaging. b) PA images of healthy and WD mice urine samples and c) corresponding PA_{970}/PA_{1260} ratio values. d) Schematic illustration of quantitative detection of human urinary Cu^{2+} by ratiometric PA imaging. e) PA images of healthy and WD patient urine samples and f) corresponding PA_{970}/PA_{1260} ratio values. g) Comparison of human urinary Cu^{2+} contents by ratiometric PA imaging and medical laboratory testing report. h) Urinary Cu^{2+} diagnostic cutoff value in clinic and corresponding PA ratio cutoff value.

© 2021 Wiley-VCH GmbH

within a few minutes) for the quantitative detection of urine Cu^{2+}. And more significantly, by reading the PA ratio, we can preliminarily determine whether the person tested is a WD patient. For example, urinary Cu^{2+} diagnostic cutoff value in clinic for normal people is <40 μg/24 h, for asymptomatic children is 40–100 μg/24 h, for WD patient is >100 μg/24 h,[25,26] corresponding PA ratio threshold are <0.809, 0.809–0.815, >0.815, respectively (Figure 4h). Thus, ratiometric PA imaging based on the nanoprobe is potential to be applied in the clinic to rapidly, quantitatively detect the Cu^{2+} in the urine of the WD patient.

After demonstrating the diagnostic capability of the designed probe in clinical urine samples, we next adapted this technique for in vivo visualization of Cu^{2+} in liver. Prior to in vivo PA imaging, the physiological stability of AuNR-Pd@PIR970/PEG nanoprobe was investigated, and no obvious aggregation was observed in various physiological solutions, indicating their excellent stability (Figure S13, Supporting Information). In addition, the cytotoxicity of the nanoprobe was examined in human hepatocellular carcinomas (HepG2) cells by CCK8 assay (Figure S14, Supporting Information). The results demonstrated that AuNR-Pd@PIR970/PEG nanoprobe (0–200 μg mL^{-1}) had negligible cytotoxicity toward HepG2 cells after incubation for 24 h. For in vivo experiment, the nanoprobe was almost cleared out from the body at 10 days post-injection (Figure S15, Supporting Information), due to relatively small size and high surface density of PEG. In addition, hematoxylin and eosin staining images of the organs including heart, liver, spleen, lung, kidney showed that there was no obvious tissue damage in the probe-treated mice compared to the control group (Figure S16, Supporting Information). These results demonstrated that the nanoprobe was biocompatible for in vivo imaging applications.

Next, we further evaluated the feasibility for quantitative detection and visualization of the liver Cu^{2+} in WD mouse model (**Figure 5**a). WD mice and healthy mice were intravenously injected (i.v.) with AuNR-Pd@PIR970/PEG nanoprobe (2.5 mg kg^{-1}). As shown in Figure 5b, both PA intensity increment at 970 nm (ΔPA_{970}) and 1260 nm (ΔPA_{1260}) gradually increased with time in WD mice until its plateau was achieved at 4 h (Figure 5d). For the healthy mice, both ΔPA_{970} and ΔPA_{1260} reached plateau at 2 h (Figure 5c) likely due to higher body metabolism rate and better liver function in healthy mice over WD mice. The maximum of ΔPA_{1260} intensity for both healthy mice and WD mice were very close (0.59, 0.55), while that of ΔPA_{970} intensity in WD mice was ≈5.53-fold higher than that of healthy mice, which was attributed to increased absorption of IR970 in response to hyperaccumulated liver Cu^{2+} in WD mice. In addition, similar to the ΔPA_{970}, the in vivo ratiometric PA signal ($\Delta PA_{970}/\Delta PA_{1260}$) of WD mice increased over time and reached its plateau (17.6) at 3 h post-injection of AuNR-Pd@PIR970/PEG (Figure 5e). For healthy mice, the $\Delta PA_{970}/\Delta PA_{1260}$ value increased over time and reached its plateau (2.96) at 2 h post-injection (Figure 5g), which is much lower than that in WD mice (Figure 5f). These results demonstrated the $\Delta PA_{970}/\Delta PA_{1260}$ of healthy mice dominated by probe accumulation in liver; $\Delta PA_{970}/\Delta PA_{1260}$ of WD mice dominated by not only probe accumulation but also probe activation by Cu^{2+}. The liver Cu^{2+} contents were calculated to be 275.1 ± 6.8 μg g^{-1} in WD mice and 25.0 ± 4.6 μg g^{-1} in healthy mice, respectively, which is in accordance with the results quantified by ICP-MS (294.8 ± 3.5 μg g^{-1} for WD mice and 29.4 ± 0.5 μg g^{-1} for healthy mice) (Figure 5i).

After verifying that the PA imaging technique could be used to quantitatively detect liver Cu^{2+} content of WD mice, we further evaluated the potential of this technique in clinical diagnosis. Currently, liver biopsy is a common clinical choice for measuring liver Cu^{2+} content, while its accuracy and invasion remain controversial.[27] If the volume of the liver can be measured noninvasively, combined with the liver Cu^{2+} concentration obtained by PA imaging technique, the liver Cu^{2+} content can be obtained. This will provide a feasible method for noninvasive detection of liver Cu^{2+}. Fortunately, the Vevo LAZR-X PA imaging system (Visual-Sonics Co. Ltd., Toronto, Canada) with 3D imaging function enables measure the volume of liver via multi-slice reconstruction method (Figure S17, Supporting Information). For example, the volume of the WD mouse liver measured by 3D imaging technique was 1.486 cm^3, very close to that measured by graduated flask (1.50 cm^3). Furthermore, the 3D PA imaging system can allow the Cu^{2+}-responsive PA signal in different scan distance to be visualized, thus indirectly observing the distribution of liver Cu^{2+} (**Figure 6**a and Figure S18, Supporting Information), and showing a scan distance-dependent distribution relation (Figure 6b), which provides intuitive information for disease diagnosis. These results suggested that the activatable nanoprobe with PA imaging technique is a promising translatable method for detecting and visualizing liver Cu^{2+}.

Finally, we performed comparison of the performance of ratiometric PA imaging with liver biopsy in the liver Cu^{2+} detection (Figure 6c,d). Liver biopsy have the following shortcomings: 1) invasive and risky, 2) the Cu^{2+} distribution of liver is not uniform, and the collected sample is small, hence leading to the potential large error, 3) complicated procedures, including biopsy, drying, weighing, digestion, spectrum analysis, etc., any step may cause measurement errors and affect the results of the detection, 4) long waiting time for reports (around a few days), as shown in Figure 6d. Compared to the liver biopsy, the established ratiometric PA imaging technique has the following advantages: 1) noninvasive, 2) image of the Cu^{2+} in the entire liver, thus reducing the error, 3) simple procedures, only the probe injection is needed, and the value can be analyzed after imaging, 4) short waiting time for reports. Therefore, ratiometric PA imaging technique can provide a promising candidate for the early diagnosis of WD.

3. Conclusion

In summary, we developed an NIR-II ratiometric PA nanoprobe (AuNR-Pd@PIR970/PEG) to rapidly, noninvasively, and quantitatively detect urinary Cu^{2+} and in vivo visualize WD-involved Cu^{2+} accumulation in the liver of living mice. AuNR-Pd@PIR970/PEG nanoprobe was consisted of NIR PA contrast reagent (IR970) that was selectively reactive to Cu^{2+} and inert inorganic AuNR-Pd with strong absorption peak at

© 2021 Wiley-VCH GmbH

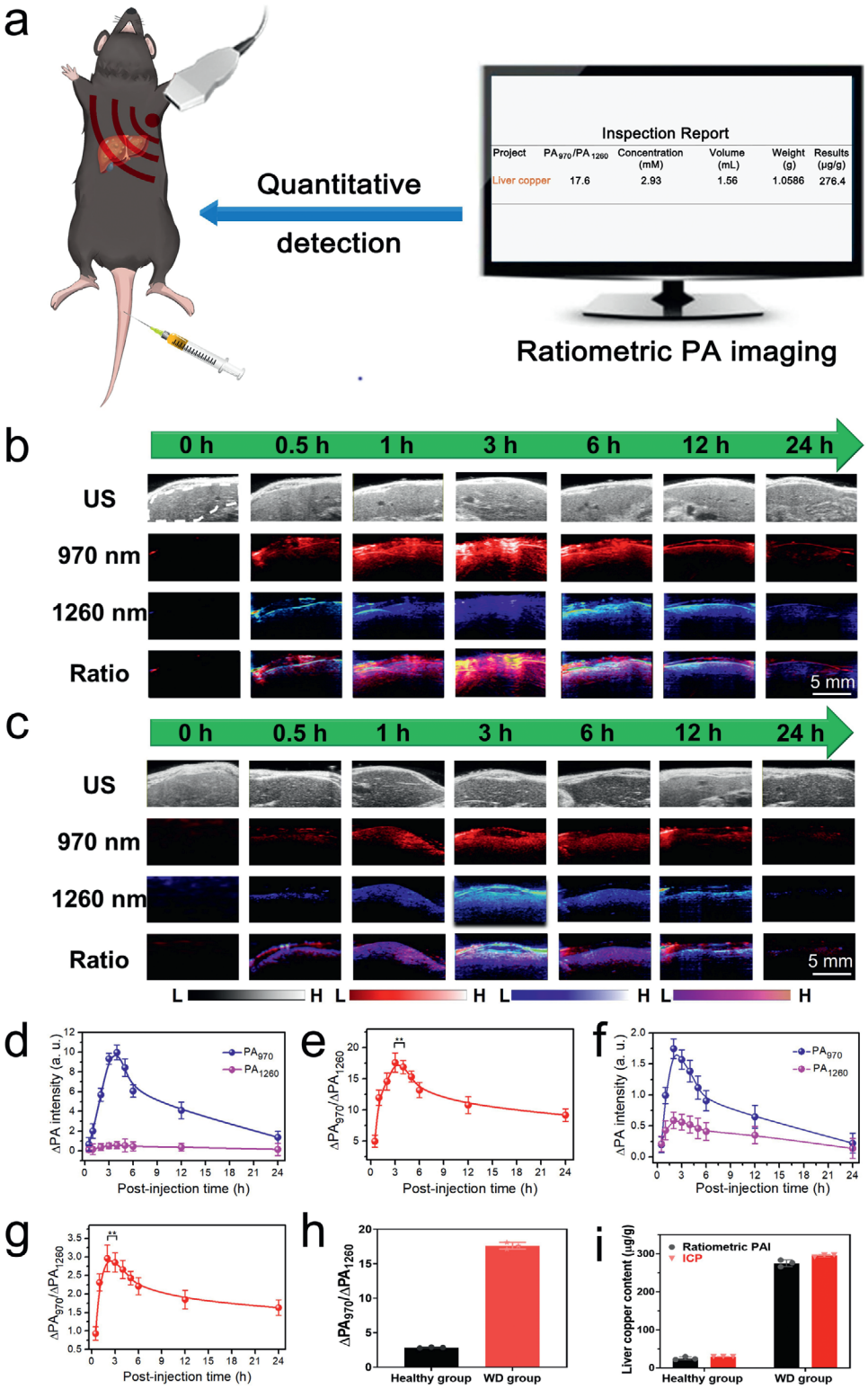

Figure 5. a) Schematic illustration of mice liver Cu^{2+} quantitative detection by ratiometric PA imaging. b) Ultrasonic (B-mode) and PA images of mice liver with WD and c) healthy mice. d) Corresponding PA intensity at 970, 1260 nm and e) PA_{970}/PA_{1260} value in WD group. f) Corresponding PA intensity at 970, 1260 nm and g) PA_{970}/PA_{1260} peak value in healthy group. h) PA_{970}/PA_{1260} value. i) Liver Cu^{2+} contents measured by liver biopsy and ratiometric PA imaging of healthy and WD mice.

© 2021 Wiley-VCH GmbH

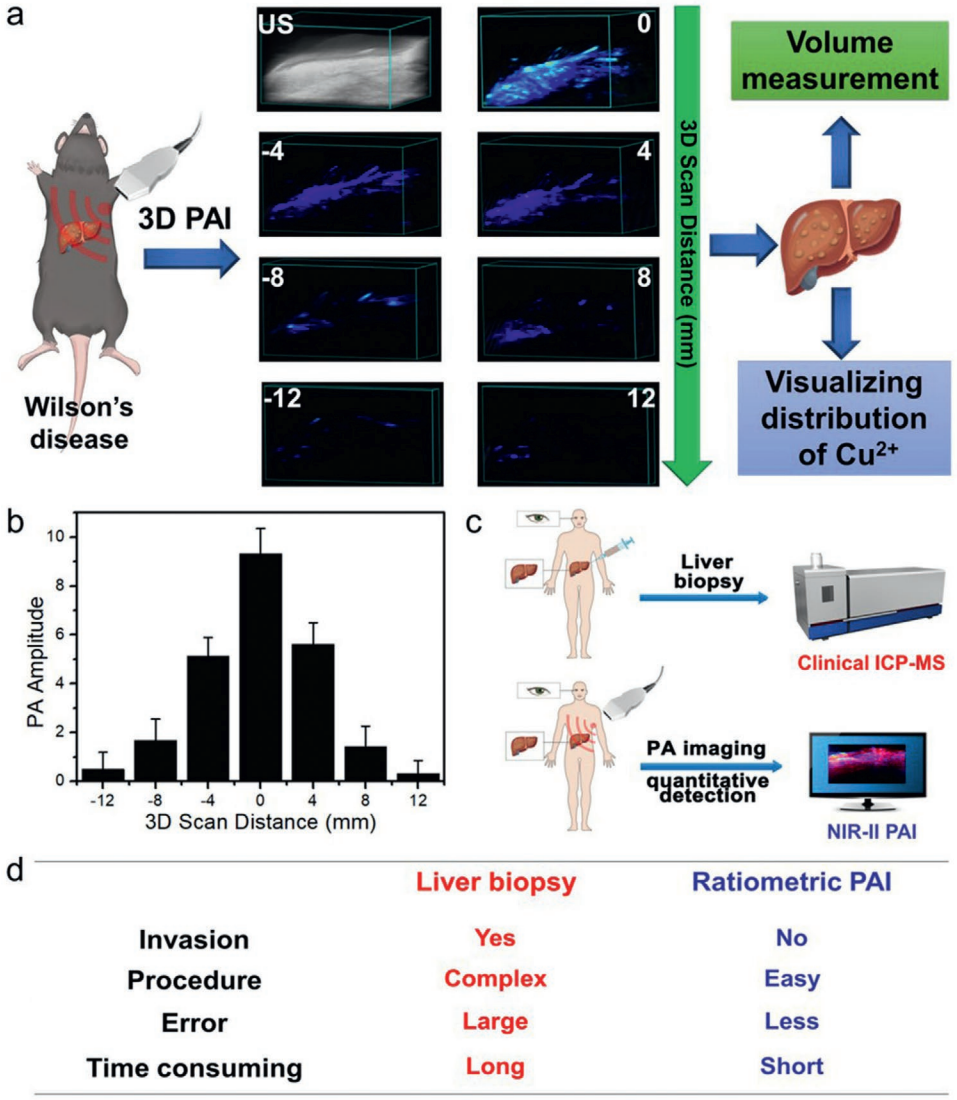

Figure 6. a) Schematic illustration of volume measurement of liver and visualizing distribution of liver Cu^{2+} by 3D PA imaging. b) PA_{970} amplitude of different 3D scan distance. c) Schematic illustration of liver Cu^{2+} detection methods by liver biopsy in clinic and PA imaging technique. d) Comparison of the performance of ratiometric PA imaging with liver biopsy in the liver Cu^{2+} detection.

1260 nm, thus achieving ratiometric PA (PA_{970}/PA_{1260}) detection of Cu^{2+}. The ratiometric nanoprobe with PA imaging technique showed the following advantages: i) The nanoprobe displayed wide liner response range and low detection limit. ii) It could be used to quantitatively detect urinary Cu^{2+} of WD patient with rapidity, high sensitivity, and accuracy; the detection results were substantially consistent with the current assays, further emphasizing the potential in clinic translation. iii) The nanoprobe could quantitatively detect liver Cu^{2+} content and visually track Cu^{2+} distribution in liver by PA imaging techniques, thus it avoided the body injury, complex procedures, error, and long waiting time during the clinical Cu^{2+} test using liver biopsy method. Overall, this ratiometric PA detection method provides a noninvasive technique with precision, celerity, and simplification, which could be considered as a promising tool for the early diagnosis of WD.

Supporting Information

Supporting Information is available from the Wiley Online Library or from the author.

Acknowledgements

This work was supported by the National Natural Science Foundation of China (nos. 21874024, 21635002) and the joint research projects of Health and Education Commission of Fujian Province (no. 2019-WJ-20). All surgical interventions and postoperative animal care were approved by the Institutional Animal Care and Use Committee of the Fujian Medical University. In addition, all experimental animal methods were carried out according to the guide for the care and use of laboratory animals (Ministry of Science and Technology of China, 2013).

Conflict of Interest

The authors declare no conflict of interest.

© 2021 Wiley-VCH GmbH

Data Availability Statement

Research Data are not shared.

Keywords

biosensing, NIR-II, photoacoustic imaging, ratiometric nanoprobe, Wilson's disease

Received: December 23, 2020
Revised: January 22, 2021
Published online:

[1] A. Czlonkowska, T. Litwin, P. Dusek, P. Ferenci, S. Lutsenko, V. Medici, J. K. Rybakowski, K. H. Weiss, M. L. Schilsky, *Nat. Rev. Dis. Primers* **2018**, *4*, 21.
[2] S. Lee, G. Barin, C. M. Ackerman, A. Muchenditsi, J. Xu, J. A. Reimer, S. Lutsenko, J. R. Long, C. J. Chang, *J. Am. Chem. Soc.* **2016**, *138*, 7603.
[3] Y. Liu, Q. Su, M. Chen, Y. Dong, Y. Shi, W. Feng, Z. Y. Wu, F. Li, *Adv. Mater.* **2016**, *28*, 6625.
[4] J. Huang, K. Pu, *Angew. Chem., Int. Ed.* **2020**, *59*, 11717.
[5] Q. Fu, R. Zhu, J. Song, H. Yang, X. Chen, *Adv. Mater.* **2019**, *31*, 1805875.
[6] Q. Li, S. Li, S. He, W. Chen, P. Cheng, Y. Zhang, Q. Miao, K. Pu, *Angew. Chem., Int. Ed.* **2020**, *59*, 7018.
[7] Y. Cai, Z. Wei, C. Song, C. Tang, W. Han, X. Dong, *Chem. Soc. Rev.* **2019**, *48*, 22.
[8] J. Zhou, Y. Jiang, S. Hou, P. K. Upputuri, D. Wu, J. Li, P. Wang, X. Zhen, M. Pramanik, K. Pu, H. Duan, *ACS Nano* **2018**, *12*, 2643.
[9] S. Wang, Z. Sheng, Z. Yang, D. Hu, X. Long, G. Feng, Y. Liu, Z. Yuan, J. Zhang, H. Zheng, X. Zhang, *Angew. Chem., Int. Ed.* **2019**, *58*, 12415.
[10] G. Ku, M. Zhou, S. Song, Q. Huang, J. Hazle, C. Li, *ACS Nano* **2012**, *6*, 7489.
[11] I.-T. Ho, J. L. Sessler, S. S. Gambhir, J. V. Jokerst, *Analyst* **2015**, *140*, 3731.
[12] S. Roberts, M. Seeger, Y. Jiang, A. Mishra, F. Sigmund, A. Stelzl, A. Lauri, P. Symvoulidis, H. Rolbieski, M. Preller, X. L. Deán-Ben, D. Razansky, T. Orschmann, S. C. Desbordes, P. Vetschera, T. Bach, V. Ntziachristos, G. G. Westmeyer, *J. Am. Chem. Soc.* **2018**, *140*, 2718.
[13] Z. Yang, Y. Dai, C. Yin, Q. Fan, W. Zhang, J. Song, G. Yu, W. Tang, W. Fan, B. C. Yung, J. Li, X. Li, X. Li, Y. Tang, W. Huang, J. Song, X. Chen, *Adv. Mater.* **2018**, *30*, 1707509.
[14] W. Huang, R. Chen, Y. Peng, F. Duan, Y. Huang, W. Guo, X. Chen, L. Nie, *ACS Nano* **2019**, *13*, 9561.
[15] X. Huang, J. Song, B. C. Yung, X. Huang, Y. Xiong, X. Chen, *Chem. Soc. Rev.* **2018**, *47*, 2873.
[16] J. Zhang, X. Zhen, P. K. Upputuri, M. Pramanik, P. Chen, K. Pu, *Adv. Mater.* **2017**, *29*, 1604764.
[17] K. Zhang, X. Meng, Z. Yang, Y. Cao, Y. Cheng, D. Wang, H. Lu, Z. Shi, H. Dong, X. Zhang, *Adv. Mater.* **2019**, *31*, 1807888.
[18] Y. Liu, S. Wang, Y. Ma, J. Lin, H.-Y. Wang, Y. Gu, X. Chen, P. Huang, *Adv. Mater.* **2017**, *29*, 1606129.
[19] S. Wang, G. Yu, Y. Ma, Z. Yang, Y. Liu, J. Wang, X. Chen, *ACS Appl. Mater. Interfaces* **2019**, *11*, 1917.
[20] H. Li, P. Zhang, L. P. Smaga, R. A. Hoffman, J. Chan, *J. Am. Chem. Soc.* **2015**, *137*, 15628.
[21] J. Ye, Z. Li, Q. Fu, Q. Li, X. Zhang, L. Su, H. Yang, J. Song, *Adv. Funct. Mater.* **2020**, *30*, 2001771.
[22] L. Zeng, G. Ma, H. Xu, J. Mu, F. Li, X. Gao, Z. Deng, J. Qu, P. Huang, J. Lin, *Small* **2019**, *15*, 1803866.
[23] K. Kiyose, H. Kojima, Y. Urano, T. Nagano, *J. Am. Chem. Soc.* **2006**, *128*, 6548.
[24] L. W. Gray, F. Peng, S. A. Molloy, V. S. Pendyala, A. Muchenditsi, O. Muzik, J. Lee, J. H. Kaplan, S. Lutsenko, *PLoS One* **2012**, *7*, e38327.
[25] O. Bandmann, K. H. Weiss, S. G. Kaler, *Lancet Neurol.* **2015**, *14*, 103.
[26] E. Nicastro, G. Ranucci, P. Vajro, A. Vegnente, R. Iorio, *Hepatology* **2010**, *52*, 1948.
[27] X. Yang, X. P. Tang, Y. H. Zhang, K. Z. Luo, Y. F. Jiang, H. Y. Luo, J. H. Lei, W. L. Wang, M. M. Li, H. C. Chen, S. L. Deng, L. Y. Lai, J. Liang, M. Zhang, Y. Tian, Y. Xu, *Hepatology* **2015**, *62*, 1731.

© 2021 Wiley-VCH GmbH